HIGH-RESOLUTION SIMULATIONS OF THE REIONIZATION OF AN ISOLATED MILKY WAY–M31 GALAXY PAIR

P. OCVIRK[1], D. AUBERT[1], J. CHARDIN[1], A. KNEBE[2], N. LIBESKIND[3], S. GOTTLÖBER[3], G. YEPES[2], AND Y. HOFFMAN[4]

[1] Observatoire Astronomique de Strasbourg, 11 rue de l'Université, F-67000 Strasbourg, France
[2] Grupo de Astrofísica, Departamento de Fisica Teorica, Modulo C-8, Universidad Autónoma de Madrid, Cantoblanco E-280049, Spain
[3] Leibniz-Institute für Astrophysik Potsdam (AIP), An der Sternwarte 16, D-14482 Potsdam, Germany
[4] Racah Institute of Physics, Hebrew University, Jerusalem 91904, Israel

ABSTRACT

We present the results of a set of numerical simulations aimed at studying reionization at the galactic scale. We use a high-resolution realization of the formation of the Milky Way (MW)–M31 system to simulate the reionization of the Local Group. The reionization calculation was performed with the post-processing radiative transfer code ATON and the underlying cosmological simulation was performed as part of the CLUES project (http://www.clues-project.org). We vary the source models to bracket the range of source properties used in the literature. We investigate the structure and propagation of the galactic ionization fronts by a visual examination of our reionization maps. Within the progenitors, we find that reionization is patchy and proceeds locally inside-out. The process becomes patchier with decreasing source photon output. It is generally dominated by one major H II region and one to four additional isolated smaller bubbles, which eventually overlap. Higher emissivity results in faster and earlier local reionization. In all models, the reionization of the MW and M31 are similar in duration, i.e., between 203 Myr and 22 Myr depending on the source model, placing their z_{reion} between 8.4 and 13.7. In all models except the most extreme, the MW and M31 progenitors reionize internally, ignoring each other despite being relatively close to each other, even during the epoch of reionization. Only in the case of strong supernova feedback suppressing star formation in halos less massive than $10^9\,M_\odot$, and using our highest emissivity, do we find that the MW is reionized by M31.

Key words: cosmology: theory – galaxies: formation – galaxies: high-redshift – intergalactic medium – methods: numerical – radiative transfer

Online-only material: color figures

1. INTRODUCTION

In the last decade, the epoch of reionization (hereafter EoR) has received increasing attention. Most observational works now seem to converge on reionization beginning as early as $z = 15$ (Kogut et al. 2003) and finishing around $z = 6$ (Fan et al. 2006), in apparent agreement with theoretical expectations (Haardt & Madau 2011). Reionization also affects the way galaxies form: it has been suggested that the rising metagalactic UV radiation field is responsible for evaporating the gas of low-mass galaxies (Gnedin 2000; Hoeft et al. 2006), affecting their star formation and therefore also the buildup of the galactic halo (Bekki & Chiba 2005). This seems to provide a credible solution to the "missing satellites problem" (Klypin et al. 1999; Moore et al. 1999) by inhibiting star formation in low-mass galaxies at early times (Bullock et al. 2000; Benson et al. 2002a, 2002b, 2003). In this framework, a number of simple semi-analytical models (hereafter SAMs) have been shown to reproduce well the satellite population of the Milky Way (hereafter MW), such as those by Koposov et al. (2009), Muñoz et al. (2009), Busha et al. (2010), Macciò et al. (2010), Li et al. (2010), and Font et al. (2011). They suggest that the ultra-faint dwarf galaxies (hereafter UFDs) discovered by the Sloan Digital Sky Survey (Martin et al. 2004; Willman et al. 2005; Zucker et al. 2006; Belokurov et al. 2007; Irwin et al. 2007; Walsh et al. 2007) are effectively reionization fossils, living in sub-halos of about $10^{6-9}\,M_\odot$. More recently, Ocvirk & Aubert (2011, 2012) showed that the structure of the UV background during reionization has a strong impact on the properties of

the satellite population of galaxies. In particular, they showed that an internally driven reionization led to significant changes in the radial distribution of satellites. It is therefore of prime importance to determine how inhomogeneous the UV field is within an MW progenitor during reionization in a realistic setting. It has been shown that at least at large scales, reionization is a highly patchy process (Zahn et al. 2007; Aubert & Teyssier 2010). However, little is known about how reionization proceeds at galactic scales. For instance, is it driven by internal or external sources? Weinmann et al. (2007), Alvarez et al. (2009), and Iliev et al. (2011, hereafter I11) attempted to describe reionization at the galactic scale, but focused on rather large volumes in order to account for large, rare overdensities such as galaxy clusters and groups, which produce the earliest sources. In these studies, the spatial resolution of the radiative transfer (hereafter RT) grid was $0.25–1\,h^{-1}$ Mpc, which does not allow a detailed study of the ionization fronts (hereafter I-fronts) propagation *within* an MW progenitor. Moreover, the Milky Way environment also comprises the nearby, massive Andromeda galaxy. Therefore, despite these previous studies, a number of questions are left open, including the following.

1. What is the influence of our neighbor M31 on the reionization of our Galaxy?
2. What is the structure of the UV field at galactic scales? Approximately isotropic and/or symmetric, or very inhomogeneous?

Here we address these questions by focusing on a small volume containing the progenitors of the major Local Group (hereafter

LG) galaxies (MW, M31, and M33). We simulate its reionization with a 21 h^{-1} kpc spatial resolution to gain insight into the development and overlap of I-fronts inside the volume of the MW progenitor and its direct neighborhood. The paper is laid out as follows. First, we describe the simulation used and the radiative post-processing technique (Section 2). We then proceed to our results (Section 3) and discuss them (Section 4) before presenting our conclusions.

2. METHODOLOGY

In this paper, we use a radiative post-processing method. An N-body smoothed particle hydrodynamics (SPH) simulation of cosmic structure formation provides the gas distribution and ionizing sources distribution. These are the inputs to the radiative transfer code ATON (Aubert & Teyssier 2008), which computes the propagation of the photons and the evolution of the ionized fraction of the gas.

2.1. The CLUES Simulation

The simulation used in this work was performed in the framework of the CLUES project (Gottlöber et al. 2010).[5] It was run using standard Lambda cold dark matter (ΛCDM) initial conditions assuming a *WMAP*3 cosmology (Spergel et al. 2007), i.e., $\Omega_m = 0.24$, $\Omega_b = 0.042$, and $\Omega_\Lambda = 0.76$. A power spectrum with a normalization of $\sigma_8 = 0.73$ and a slope of $n = 0.95$ was used. The PMTree-SPH MPI code GADGET2 (Springel 2005) was used to simulate the evolution of a cosmological box with a side length of 64 h^{-1} Mpc. Within this box, a model LG that closely resembles the real LG was identified using a 1024^3 particle run (see Libeskind et al. 2010). This LG was then re-sampled with 64 times higher mass resolution in a region of 2 h^{-1} Mpc about its center, giving an equivalent resolution of 4096^3 particles, i.e., a mass resolution of $m_{\rm dm} = 2.1 \times 10^5 \, h^{-1} \, M_\odot$ for the dark matter (DM) and $m_{\rm gas} = 4.42 \times 10^4 \, h^{-1} \, M_\odot$ for the gas particles. For more details we refer the reader to Gottlöber et al. (2010). The feedback and star formation prescriptions of Springel & Hernquist (2003) were used. Outputs are written, on average, every 30 Myr. The simulation starts at $z = 50$. As it runs, DM and gas collapse into sheets and filaments extending between halos, as comprehensively described in Ocvirk et al. (2008), Codis et al. (2012), Hoffman et al. (2012), and Libeskind et al. (2012). These feed proto-galaxies which then start forming stars. It includes a uniform rising UV cosmic background generated from quasi-stellar objects and active galactic nuclei (Haardt & Madau 1996), switched on at $z = 6$. Therefore the radiative transfer computations that we perform will be valid only at earlier times. We will see that this is not a problem, since our models always achieve complete reionization before $z = 6$. This simulation has been used to investigate a number of properties of galaxy formation at high resolution (Forero-Romero et al. 2011; Knebe et al. 2011a, 2011b; Libeskind et al. 2011a, 2011b). Besides being a well-studied simulation, the advantage of this data set for the present study is twofold. First of all, it produces a fairly realistic LG at $z = 0$: the MW and M31 are in the correct range of masses and separations. Second, its mass resolution in the zoomed region allows us to resolve the $10^7 \, h^{-1} \, M_\odot$ halos. This is of crucial importance in reionization studies since they are the most numerous sources of UV photons.

---

[5] Simulation seed number 186592.

2.2. Radiative Post-processing

2.2.1. ATON

ATON is a post-processing code that relies on a moment-based description of the radiative transfer equations and tracks the out-of-equilibrium ionizations and cooling processes involving atomic hydrogen (Aubert & Teyssier 2008). Radiative quantities (energy density, flux, and pressure) are described on a fixed grid and evolved according to an explicit scheme under the constraint of a Courant–Friedrich–Lewy condition (hereafter CFL). The simulations presented in this work used a mono-frequency treatment of the radiation with a typical frequency of 20.27 eV for 50,000 K blackbody spectrum. Because of the high resolution of the CLUES simulation, we do not make any correction for the clumping, as was done for the largest boxes of Aubert & Teyssier (2010). ATON has been ported on multi-GPU architecture, where each GPU handles a Cartesian sub-domain and communications are dealt with using the MPI protocol (Aubert & Teyssier 2010). By achieving an acceleration factor 80 times compared to CPUs, the CFL condition is satisfied at high resolution within short wall-clock computing times. As a consequence, no reduced speed-of-light approximation is necessary, and it may be of great importance for the timing arguments of the local reionization discussed hereafter. During the course of this work, simulations were run on segments of 8–64 GPUs on the Titane and Curie machines of the CCRT/CEA supercomputing facility, with typically 160,000 radiative time steps performed in 37 hr.

The post-processing approximation has potentially important consequences on our results, as discussed, for instance, in Baek et al. (2009) and Frank et al. (2012). While the temperature of the gas is consistently followed by ATON, the gas density is "frozen" at that given by the SPH simulation snapshots. This means that our scheme does not allow for photoevaporation, but the photo-heating does affect the radiative transfer calculations, e.g., through the temperature dependence of the recombination rates. In this sense, our scheme is "thermally coupled," which is already an important step in the direction of a more realistic treatment (Iliev et al. 2006; Pawlik & Schaye 2011). By design, self-shielding is also accounted for, and results in a later reionization of sourceless high-density regions, such as mini-halos or the cold gas filaments. However, in a fully coupled radiative-hydrodynamics simulation, the gas field reacts to the photo-heating, and can result in the dispersion of low-mass gas structures (Shapiro et al. 2004; Iliev et al. 2005, 2009). This should induce a form of self-regulation of star formation and therefore emissivity by shutting off sources in the ionized low-mass halos, as shown in Iliev et al. (2007). Even though a small number of coupled galaxy formation codes have recently been built (Petkova & Springel 2011; Rosdahl & Blaizot 2012; Finlator et al. 2011; Wise & Abel 2011), at the moment no application to the formation of the LG in a zoom simulation such as the CLUES data set we use here has been performed, mainly because of the huge computational cost involved. In any case, the impact of full coupling on our results is very likely negligible compared to uncertainties in the source efficiency, which prompts us to explore a wide range of emissivities (see Section 2.2.3).

2.2.2. Field Setup

The gas density field is projected onto a 512^3 grid with sides of 11 h^{-1} Mpc. The center of the grid is the barycenter of all the particles which end up within 300 kpc of the MW at $z = 0$.

Table 1
Properties of the Models Used

(1) Model Name	(2) Source Type	(3) Source Criterion	(4) Emissivity (photons s^{-1} h^{-1} $M_\odot$)	(5) $z_{\rm reion}^{\rm m}$ MW	(5) M31	(6) $\Delta z_{0.1}^{0.9}$ MW	(6) M31	(7) Δt (Myr) MW	(7) M31
SPH	SPH star	⋯	6.3×10^{45}	9	9.4	2.72	2.34	202	159
H42	DM halo	$T_{\rm vir} > 10^4$ K	6.8×10^{42}	8.4	8.4	2.42	2.45	203	203
H43	DM halo	$T_{\rm vir} > 10^4$ K	6.8×10^{43}	11.5	11.8	2.57	2.48	105	98
H44	DM halo	$T_{\rm vir} > 10^4$ K	4.08×10^{44}	13.6	13.7	3.2	1.8	89	54
H42 SNfb	DM halo	$M > 10^9 \, h^{-1} \, M_\odot$	6.8×10^{42}	5.8	5.8	1.47	1.49	304	299
H43 SNfb	DM halo	$M > 10^9 \, h^{-1} \, M_\odot$	6.8×10^{43}	8.3	9.3	1.5	1.37	138	109
H44 SNfb	DM halo	$M > 10^9 \, h^{-1} \, M_\odot$	4.08×10^{44}	9.1	9.7	0.55	0.32	43	22

Notes. Note that the emissivity is given in photons s^{-1} $M_\odot^{-1}$ of the mass of *young stars* for the SPH model, and of the DM halo for the halo-based models. It is given *after* accounting for an escape fraction $f_{\rm esc} = 0.2$. The H42 model has been calibrated so as to produce the same total number of photons as the SPH model at $z = 10$. Column 4 gives the mass threshold of the DM halo based source models, used to mimic various forms of feedback. Column 5 gives the reionization redshift of the MW and M31 progenitors for each model, i.e., the time when the mass-weighted ionized fraction of the progenitor shown in Figure 2 reaches 0.5. Column 6 gives the duration of the progenitors' reionization as the time spent to increase the mass-weighted ionized fraction $\langle x \rangle^{\rm m}$ from 0.1 to 0.9. Column 7 gives this duration in Myr.

This setup gives us a spatial resolution of $\Delta x = 21 \, h^{-1}$ kpc. The sources are projected on the same grid. As explained in Section 2.1, the CLUES simulation uses a zoom technique, with high- and low-resolution domains. The high-resolution (hereafter HR) domain contains the objects of interest (MW and M31), and is described with DM, gas, and star particles. At 512^3 resolution, all grid cells contain at least one gas particle in the HR region in the highest redshift snapshot ($z = 19.5$). On the other hand, the low-resolution (hereafter LR) domain does not have any SPH particles. Therefore, we set the gas density in the LR domain to $\rho_{\rm LR} = 10^{-2} \rho_{\rm C}$, where $\rho_{\rm C}$ is the critical density of the universe. The LR region does not contain any stars either. Photons reaching the HR/LR boundary region just leave the LG and quickly reach the edges of the computational box. There, we use transmissive boundary conditions, i.e., light just exits the box.

2.2.3. Ionizing Source Models

We use different source models based on either the star particles spawned by the hydrodynamical star formation prescriptions of the CLUES simulation, or DM halos. We use a constant $f_{\rm esc} = 0.2$, which is among the values allowed by recent studies on the UV continuum escape fraction of high-z galaxies (Wise & Cen 2009; Razoumov & Sommer-Larsen 2010; Yajima et al. 2011). We neglect any possible active galactic nucleus phases of our emitters. Such sources could already be in place in rare massive proto-clusters during reionization (Dubois et al. 2011, 2012) and contribute to the cosmic budget of ionizing photons (Haardt & Madau 2011), but they are beyond the scope of the present study. The properties of our source models are summarized in Table 1.

SPH stars. In this model, our sources are the star particles formed in the CLUES simulation. At each time step, we select all star particles younger than 60 Myr. We use the ionizing luminosity of Table 2 of Baek et al. (2009), simulation S20. While the massive stars responsible for this radiation would have a typical lifetime of 10 Myr, we dilute their emission over 60 Myr in order to reduce the stochastic nature of star particle spawning in the simulation. Each star particle weighs $m_\star = 2.21 \times 10^4 \, h^{-1} \, M_\odot$. It is therefore more representative of a "cluster" of stars, and results in 1.9×10^{50} ionizing photons s^{-1} delivered to the intergalactic medium (IGM) for 60 Myr, after accounting for $f_{\rm esc} = 0.2$.

Because of the large mass of the star particles and the slow pace of star formation during the EoR, we cannot guarantee that the star formation rate (SFR) is converged in the numerical sense (Springel & Hernquist 2003; Rasera & Teyssier 2006), and as a consequence some sites of early star formation may be missing. Moreover, Chardin et al. (2012) showed that the topology of H II regions during the EoR could be strongly affected by this issue. Therefore we also consider source models based on DM halos.

Halo sources. As an alternative to the direct use of SPH stars, we here use DM halos as sources. They are detected using the Amiga halo finder (Gill et al. 2004; Knollmann & Knebe 2009). We keep only the halos that have more than 90% of their mass in high-resolution DM particles. Dwarf galaxies of the early universe are subject to a wide range of feedback processes beyond photoevaporation by a UV background. Although our code does not allow for live self-regulation of the sources, we tried to account for the influence of at least some of the relevant feedback processes.

External Lyman–Werner background. Massive stars radiate in the Lyman–Werner (LW) band, which, contrary to H-ionizing photons, can travel several tens of Mpc through neutral hydrogen (Barkana & Loeb 2001; Ahn et al. 2009). Therefore, it is legitimate to consider that our computational domain containing the LG must see the LW radiation of the earliest, rare sources of the universe. It has been shown that the stellar LW background can be sufficiently strong to dissociate molecular hydrogen, which is the main coolant of pristine low-mass halos below $T_{\rm vir} = 10^4$ K, therefore suppressing star formation. This can happen very early during the EoR, as early as $z = 12$ according to Ahn et al. (2009, 2012). However, the latter is an average value, and it is only natural to expect that the LW background rises faster in overdensities such as the LG, all the more so in the neighborhood of a massive cluster such as Virgo. Therefore, we consider that only the atomic cooling halos in our box are able to form stars. Following Iliev et al. (2002), we consider that halos need to have a virial temperature $T_{\rm vir} > 10^4$ K in order to do so. We use their formula to compute the minimum mass required for a halo to be an atomic cooling source. It gives roughly $1.4 \times 10^7 \, h^{-1} \, M_\odot$ at $z = 20$ and about $1 \times 10^8 \, h^{-1} \, M_\odot$ at $z = 5$, which is the time spanned by our radiative post-processing simulation. In this model, only the halos above this mass are emitting. We assign an instantaneous SFR to each halo, assuming SFR $\propto M$. Note that in our framework, unlike in I11, sources are not regulated, i.e., above the mass threshold;
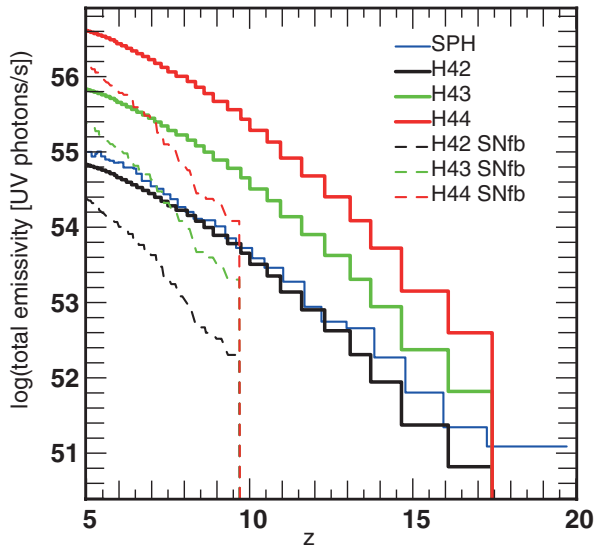
Figure 1. Total emissivities of the sources in the 11 h^{-1} Mpc radiative transfer box for our seven models.

(A color version of this figure is available in the online journal.)

they emit continuously as long as the halo exists. In order to be able to compare the SPH and halo-based models we calibrated the emissivity of the halos of the H42 model so that the total number of UV photons emitted at $z = 10$ is the same in both models. With this calibration, the total photon output evolution of the two models is quite similar, although SPH is slightly more luminous, as can be seen in Figure 1. Accounting for a constant $f_{esc} = 0.2$, our calibration gives for H42

$$\dot{N}_\gamma/M = 6.8 \times 10^{42} \text{ photons s}^{-1} M_\odot^{-1}. \quad (1)$$

The emissivities of the other models are listed in Table 1, and their total photon outputs are shown in Figure 1 as well. In our units, the low (high) efficiency assumptions of I11 give about 4–$6 \times 10^{42-43}$ (4×10^{43}–1×10^{44}) photons s^{-1} $M_\odot^{-1}$. Therefore the range of emissivities explored here roughly brackets the scenarios considered in I11 and extends to the lower efficiency scenario of Baek et al. (2009). These have been shown to produce viable reionization histories in their respective contexts, and are therefore used here as guidance, although the much smaller halos are more abundant.

Strong feedback from supernovae. Stellar feedback processes in galaxies are expected to affect star formation, but are generally poorly constrained. Supernovae, for instance, by blowing away and/or heating their host galaxy's cold gas reservoir, have been shown to be potentially very important for the evolution of low-mass galaxies (Benson et al. 2003). The details of supernova feedback and the galaxy mass at which it kicks in depend on a wide range of parameters (stellar rotation and chemical composition determining supernova energy production, mechanical coupling to the host's gas, host DM density profile, gas metallicity, and its cooling properties) and have been hotly debated since the study of Dekel & Silk (1986). At low redshift, some insight can be gleaned thanks to direct observation of the interaction between supernova ejecta or superbubbles and their host's gas. Such observations are not available at high redshift, let alone during the EoR. Indeed, supernova feedback at high z could be quite different from what we see at low z (Barkana & Loeb 2001). Recent semi-analytical models of galaxy formation (Kim et al. 2013) during the EoR have shown that

supernovae feedback could render star formation in low-mass galaxies ($V_{circ} < 30$ km s^{-1}) so inefficient that their contribution to the ionizing photon budget becomes negligible (less than 1%). At the beginning of our radiative post-processing (i.e., $z = 19.35$), this corresponds to DM halos of roughly $10^9 h^{-1} M_\odot$. In order to investigate the impact of such strong supernova feedback, we designed an additional set of models, which we refer to as HXX SNfb. Following the results of Kim et al. (2013), all halos less massive than $10^9 h^{-1} M_\odot$ are assumed to be inefficiently forming stars and we set their emissivity to 0. Above this mass threshold, we assume that galaxies are allowed to continuously form stars and produce UV photons following the same emissivities as H42,43,44.[6] Because of the small number of emitters, the total photon output of this model within our box is much smaller than in the other four baseline scenarios, as can be seen in Figure 1. The figure shows that in this model, efficient sources appear only at $z < 10$, whereas the SPH model, which also includes a self-consistent supernova feedback, forms stars at all times. This readily shows that our proposed implementation of supernova feedback in the HXX SNfb models is rather extreme, which is why we refer to it as "strong" feedback. Nevertheless, we consider it as a limiting case.

3. RESULTS

First, we check the good behavior of our setup and method by analyzing the global reionization history of the two major galaxies' progenitors in the box. Then, we produce reionization maps to investigate how reionization proceeded spatially within the progenitors for our sets of models.

3.1. Global Progenitor Reionization History

The DM particles that end up within 300 h^{-1} kpc of the MW center at $z = 0$ are located in a sphere of $\sim 1 h^{-1}$ Mpc comoving radius at $z = 19.35$. Their detailed distribution is not exactly spherical but the 1 h^{-1} Mpc sphere remains a good approximation of it. This defines our MW progenitor volume, and we proceed similarly for M31. The evolution of the mass-weighted ionized fraction within the progenitor is shown in Figure 2 for our H42-44 and SPH baseline models. Depending on source emissivity, the reionization of the progenitors is achieved between $z = 7.5$ and $z = 14$. The difference in reionization histories due to the different emissivities is always much larger than the difference between MW and M31 reionization histories. All models produce a very smooth and monotonous reionization of the progenitors. The timings and trends with emissivity are in fair agreement with a number of recent studies, such as Li et al. (2013). The bottom panel of Figure 2 shows the ratio of the mass-weighted to the volume-weighted ionized fraction. For the SPH, H42, and H43 models, $\langle x \rangle^m / \langle x \rangle^v > 1$ for most of the redshift range, indicating that high-density regions are more ionized than low-density regions, i.e., I-front propagation proceeds locally inside-out: high-density regions containing the sources are reionized first and the neighboring regions with lower densities are impacted only later on. The ratio drops below unity as voids become dominant in ionized regions before reaching unity as sourceless denser regions such as gas filaments (Finlator et al. 2009) are eventually reionized. The maximum of $\langle x \rangle^m / \langle x \rangle^v$ (i.e., early times) drops with increasing emissivity,

---

[6] To prevent any confusion, we here remind the reader that this strong feedback process operates exclusively in the radiative post-processing step of our workflow. The original SPH simulation remains the same as in the baseline H42-44 and SPH models.
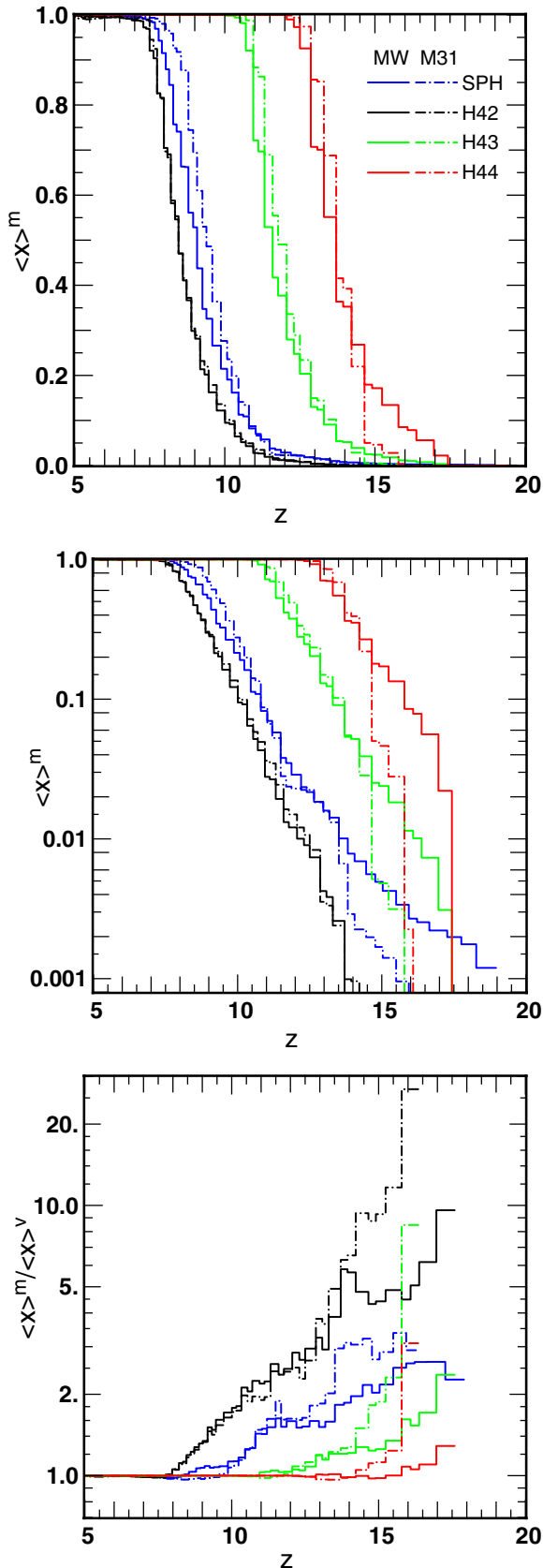
Figure 2. Ionized fractions of the MW (solid line) and M31 (dot–dashed line) progenitors for our four baseline models. Top: mass-weighted ionized fractions; middle: log scale; bottom: ratio of the mass-weighted to the volume-weighted ionized fractions $\langle x \rangle^{\mathrm{m}}/\langle x \rangle^{\mathrm{v}}$. The color and symbol codes are specified in the top panel.

(A color version of this figure is available in the online journal.)

because in the photon-poor scenarios, it takes longer for the cell hosting the source to get ionized and let the photons leak out into the low-density regions.

3.2. Reionization Maps

We determine the reionization redshift of a given cell as the redshift of the last snapshot where its neutral fraction was above $x_{\mathrm{ion}} > 0.5$, i.e., if a cell reionizes at z_1 and then recombines and gets ionized again at $z_2 < z_1$, we keep z_2 as the reionization redshift. The respective centers of the MW, M31, and M33 at $z = 6$ progenitors define a unique plane, which we will refer to as the 3M plane throughout the paper. It provides a useful common reference for studying the reionization history of these galaxies. The maps of Figure 3 show the average reionization redshift in a slab of $0.2\ h^{-1}$ Mpc thickness centered on this plane. The three red dashed circles of radius 1, 1, and $0.5\ h^{-1}$ Mpc, respectively, for MW, M31, and M33 are centered on each galaxy's center of mass at $z = 6$. They are indicative of the position and extent of each galaxy's progenitor. The sawtooth features on the sides are due to the transition from the HR to LR domain of the original hydrodynamical simulation. The maps are ordered by increasing global average reionization redshift, which also corresponds to increasing source efficiency. The color codes are set by the minimum and maximum redshifts of each map. This allows us to investigate the difference in I-front structures and propagation between the different models.

3.2.1. Impact of Source Emissivity

Low-efficiency (H42 and SPH) models are patchier than their high-efficiency counterparts (H43-44). The MW progenitor of the low-efficiency models seems to consist of four main objects which reionize in isolation. This patchiness is expected due to the multiplicity of sources within each progenitor. The patches themselves also display a lot of internal structure. The latter can be related to the presence of dense infalling gas sheets and filaments, which reionize later than diffuse regions, as shown in Finlator et al. (2009). The structures of the individual patches also become smoother with increasing source efficiency. Due to the very low density we set in the LR region, reionization happens there very quickly, driven by a few sources outside of the volume plotted here, located at the HR/LR boundary.

3.2.2. Star versus Halo Source Model

The H42 and SPH models have comparable emissivities at all times. As a result, the overall structure of their maps is rather similar: the patches are in comparable numbers and extents, except for the largest MW patch, which seems to reionize earlier in the SPH model. However, the average z_{reion} is slightly higher in the SPH model. Indeed, we have shown that the H42 model is slightly fainter and its photons are distributed upon a larger number of sources, and therefore each source is less luminous than its SPH counterpart. This small difference in luminosity is also the cause of the difference seen in the M31 region between the H42 and SPH models. For H43 and H44, the M31 region looks much more like that in the SPH model. Therefore, besides the effect described above, which could be compensated by a small increase in emissivity of the H42 model, we see that the details of source modeling play a small role: the photon output is the driving parameter here.

3.2.3. Comparison with M31 and M33

Except for the H42 model, the progenitor of M31 consists of fewer reionization patches than the MW region. However,
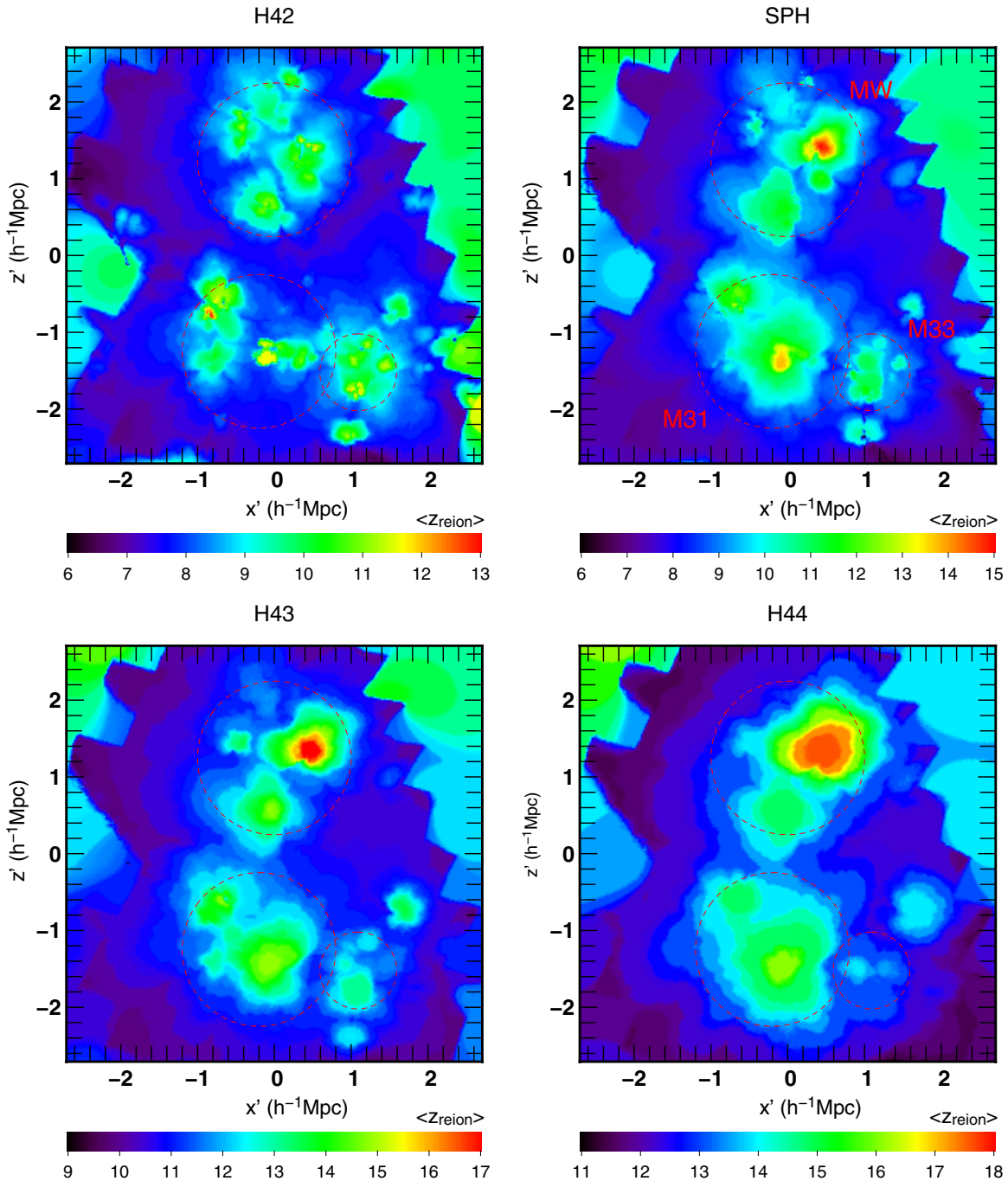
Figure 3. Reionization maps of the LG of galaxies for our four baseline models. The simulation domain has been cut in the plane containing the centers of M31, M33, and the MW. The maps are obtained as the average z_{reion} of a slab of 0.2 h^{-1} Mpc thickness centered on this plane. The color codes the reionization redshift of each cell. The red dashed circles show the approximate location of the progenitors of the three major LG galaxies. The square artifacts in the corners are due to the transition from the high- to low-resolution domains of the SPH simulation.

(A color version of this figure is available in the online journal.)

at high emissivities (H44), both objects only have two major patches. In the SPH model, reionization starts slightly earlier in the MW than in M31. Indeed, in the simulation we used, the first stars appear in larger numbers in the MW region than in M31. This trend is also seen in the H43-44 models, indicating that its origin likely lies in the slower assembly of M31 in the simulation. Such a delay in the formation of two galaxies of similar mass in a pair is not uncommon, as can be seen in Figure 2 of Forero-Romero et al. (2011) for similar simulations.

3.3. Reionization in Isolation?

In all of our baseline models (H42,43,44) and SPH, M31 and the MW ignore each other during the reionization epoch. There is always a clear gap in z_{reion} between them, and therefore the reionization of each progenitor is driven only by its inner sources. This is also true for the less massive M33, which seems to reionize a fair fraction of its progenitor in all models.

The fact that the MW and M31 did not interact radiatively during reionization could be an important simplification in
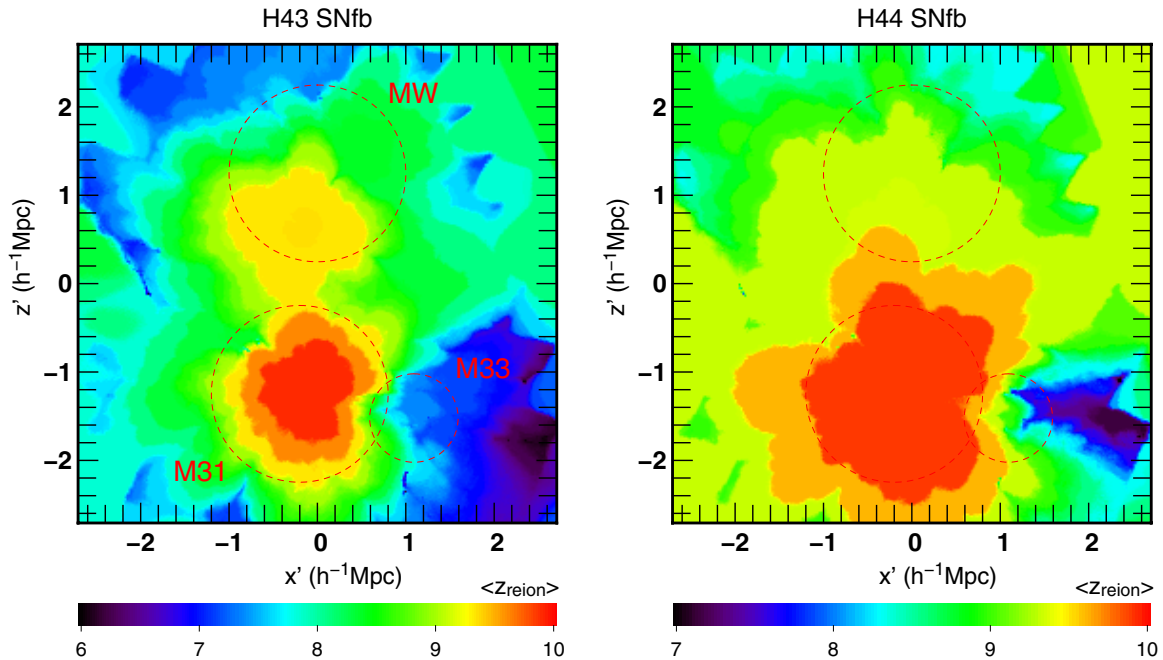
Figure 4. Same as Figure 3 for our two strong feedback scenarios. Reionization becomes very quick and is driven by a small number of sources, hence the small number of patches. In the most extreme scenario (right), M31 reionizes the MW progenitor.

(A color version of this figure is available in the online journal.)

satellite population models where no influence from Virgo is considered. This result would validate the approach used for the internal reionization models of Ocvirk & Aubert (2011), Font et al. (2011), and many more, who neglect the influence of M31 on the reionization of MW satellites.

However, in the following, we show that there is still a possibility that the MW and M31 may have influenced each other during the EoR, by analyzing our models with strong supernova feedback. The global properties of these scenarios are shown in Table 1. Since the mass threshold for continuous star formation delays the apparition of the first efficient sources, the SNfb models reionize much later than the baseline models with the same emissivity. The H42 SNfb model can be readily dismissed as unrealistic since the reionization of the MW or M31 is achieved later than $z = 6$. This model is at odds with the constraints derived from the Gunn–Peterson trough in quasar spectra (Fan et al. 2006). Moreover, a broad range of reionization models agree in predicting that the MW or M31 should have reionized earlier than the rest of the universe (Li et al. 2013; J. Chardin et al. 2013, in preparation). Therefore we consider only the two high-emissivity H43 and H44 SNfb models and compute their reionization maps as shown in Figure 4. First of all, the maps have even less structure than in the H44 baseline model. Instead of two patches, we have only one major patch in M31's and MW's progenitors in H43 SNfb and just one patch in the whole map for H44 SNfb, centered on M31. While M31's progenitor displays a clear inside-out reionization pattern in both maps, the situation is more complex for the MW's progenitor. In the H43 SNfb model, the MW region features a single patch, produced by a source that turned on much later than M31's sources. Moreover, a significant fraction of the progenitor's volume appears to reionize at the same redshift as the IGM surrounding the MW and M31. Whether the progenitor is internally or externally reionized is not so clear-cut anymore. The situation becomes unambiguous in the H44 SNfb panel: the map shows one single patch centered on M31. In this scenario,

the reionization of the LG is driven by M31 alone. The MW's progenitor is quickly, externally reionized by M31.

4. DISCUSSION

Even though most of our models yield clearly isolated reionization scenarios for the MW and M31, a radiative influence of M31 on the MW or vice versa cannot be ruled out with our current constraints on the strength of the feedback and the emissivity of the sources. Reducing the number of sources by increasing the minimum mass threshold while increasing their emissivity yields a "first source wins it all" scenario. We note, however, that this scenario is at the extreme end of our parameter range: it appears only with the strongest source suppression and highest emissivity. It is not clear if this model would produce a reasonable global reionization history in a large scale box. It would be useful to check this with a further simulation of a large volume, but this is outside of the scope of the present paper. Reviewing the literature, we did not find any study where this combination of emissivity and source minimum mass has been ruled out.

The internal, isolated reionization of MW-size galaxies found by our baseline models (H42,43,44, and SPH) is in agreement with results from Weinmann et al. (2007) and the photon-poor regime of I11. However, model 1 of I11 (roughly similar to our model H43) predicts that for high emissivities, the LG should be reionized *externally* by photons from Virgo, at $z = 10.5$–10.25. We found that in this regime the MW and M31 actually reionize much earlier than this, i.e., at $z = 11.5$–11.8, and they do so *internally*. This highlights an important caveat of the present study: since the Virgo galaxy cluster is outside of the HR region of the CLUES simulation we used, it is simply not taken into account. Moreover, our work and I11 use different setups, which makes comparing reionization timings very tricky. Furthermore, the mass resolution of our simulation is a factor of ∼50 higher than in I11. It is therefore expected that the lowest mass halos

form earlier in our simulation, providing earlier sources to reionize the LG. This is well documented in the literature. For instance, the top panel of Figure 1 in Aubert & Teyssier (2010) shows the total number of emitted photons per hydrogen atom for four different resolutions, with the same stellar emissivity for all four simulations. At $z > 10$, the 12.5 h^{-1} Mpc box can produce up to 100 times more photons than the 50 h^{-1} Mpc box. This corresponds to a factor of 64 increase in mass resolution. This is close to the difference in mass resolution between I11 and the present study. We note, however, that Aubert & Teyssier (2010) refer to a post-processing method based on using star particles as a source, and not a halo-based formalism as we do here and in I11. Furthermore, our crude implementation of feedback is based on a filtering of halos less massive than 10^7–10^8 $M_\odot$ (HXX models) and 10^9 $M_\odot$ (HXX SNfb models), which reduces the impact of increased resolution on the number of sources. Finally, considering this result, it seems reasonable to expect that $z > 10$ photon production can be boosted by a large factor as a result of improved mass resolution between I11 and our study. This boost in turn leads to an earlier reionization of the LG, despite using emissivities roughly similar to the photon-rich scenario of I11. Likewise, increasing resolution would also boost the photon output of Virgo at early times, so that its I-front could reach the LG earlier than found by I11. However, the question remains, will it happen early enough to reionize the LG externally rather than internally?. Ideally, assessing the influence of Virgo on the reionization of the LG will require a high-resolution simulation of the formation of the LG and its environment, including Virgo in the spirit of I11, but at the resolution of the present work or better. Thanks to the rapid evolution of the hardware and high-performance computing facilities, we expect this will become feasible in the coming years.

5. CONCLUSIONS

We radiatively post-processed a high-resolution simulation of the formation of the LG in order to investigate the reionization of the MW and M31 at galactic scale. We used seven different ionizing source models with various emissivities and star formation criteria to assess the impact of uncertainties on the source properties. When considering only atomic cooling halos as sources, we find that the reionization of the MW progenitor is generally patchy, with two to four major regions and a few minor ones reionizing in isolation. Increasing emissivity leads to fewer isolated patches and accelerated reionization: our most photon-poor scenario reionizes the MW progenitor at $z = 8.4$, and at $z = 13.7$ in the most photon-rich regime. Our results are in fair agreement with the available literature, although very few studies discussed reionization at these scales. In all models except the most extreme, the MW and M31 progenitors reionize in isolation, despite being relatively close to each other, even during the EoR. The corresponding reionization maps always show a clear gap in $z_{\rm reion}$ between the two progenitors. Only in the case of strong supernova feedback suppressing star formation in halos less massive than 10^9 $M_\odot$, and using the highest emissivities, do we find that the MW is reionized by M31, which hosts the first efficient source to appear in the box.

Putting our study back into the general context of galaxy formation, this work is an additional step in the investigation of the internal versus external nature of galactic reionization for the MW and M31, as a function of feedback type and source emissivity. Further effort should be made in exploring the source parameter space, along with improving feedback

models, radiative and hydrodynamical, extending this work to a larger number of realizations of the MW–M31 system, and, in particular, including the impact of Virgo. We hope this work will help build a more accurate and sensible framework for future semi-analytical models of galaxy formation during the EoR, as well as models of the satellite population of the MW and M31.

REFERENCES

Ahn, K., Iliev, I. T., Shapiro, P. R., et al. 2012, ApJL, 756, L16
Ahn, K., Shapiro, P. R., Iliev, I. T., Mellema, G., & Pen, U.-L. 2009, ApJ, 695, 1430
Alvarez, M. A., Busha, M., Abel, T., & Wechsler, R. H. 2009, ApJL, 703, L167
Aubert, D., & Teyssier, R. 2008, MNRAS, 387, 295
Aubert, D., & Teyssier, R. 2010, ApJ, 724, 244
Baek, S., Di Matteo, P., Semelin, B., Combes, F., & Revaz, Y. 2009, A&A, 495, 389
Barkana, R., & Loeb, A. 2001, PhR, 349, 125
Bekki, K., & Chiba, M. 2005, ApJL, 625, L107
Belokurov, V., Zucker, D. B., Evans, N. W., et al. 2007, ApJ, 654, 897
Benson, A. J., Frenk, C. S., Baugh, C. M., Cole, S., & Lacey, C. G. 2003, MNRAS, 343, 679
Benson, A. J., Frenk, C. S., Lacey, C. G., Baugh, C. M., & Cole, S. 2002a, MNRAS, 333, 177
Benson, A. J., Lacey, C. G., Baugh, C. M., Cole, S., & Frenk, C. S. 2002b, MNRAS, 333, 156
Bullock, J. S., Kravtsov, A. V., & Weinberg, D. H. 2000, ApJ, 539, 517
Busha, M. T., Alvarez, M. A., Wechsler, R. H., Abel, T., & Strigari, L. E. 2010, ApJ, 710, 408
Chardin, J., Aubert, D., & Ocvirk, P. 2012, A&A, 548, A9
Codis, S., Pichon, C., Devriendt, J., et al. 2012, MNRAS, 427, 3320
Dekel, A., & Silk, J. 1986, ApJ, 303, 39
Dubois, Y., Devriendt, J., Slyz, A., & Teyssier, R. 2012, MNRAS, 420, 2662
Dubois, Y., Pichon, C., Haehnelt, M., et al. 2011, MNRAS, 417, 1853
Fan, X., Strauss, M. A., Becker, R. H., et al. 2006, AJ, 132, 117
Finlator, K., Davé, R., & Özel, F. 2011, ApJ, 743, 169
Finlator, K., Özel, F., Davé, R., & Oppenheimer, B. D. 2009, MNRAS, 400, 1049
Font, A. S., Benson, A. J., Bower, R. G., et al. 2011, MNRAS, 417, 1260

Forero-Romero, J. E., Hoffman, Y., Yepes, G., et al. 2011, MNRAS, 417, 1434
Frank, S., Rasera, Y., Vibert, D., et al. 2012, MNRAS, 420, 1731
Gill, S. P. D., Knebe, A., & Gibson, B. K. 2004, MNRAS, 351, 399
Gnedin, N. Y. 2000, ApJ, 542, 535
Gottlöber, S., Hoffman, Y., & Yepes, G. 2010, arXiv:1005.2687
Haardt, F., & Madau, P. 1996, ApJ, 461, 20
Haardt, F., & Madau, P. 2011, arXiv:1103.5226
Hoeft, M., Yepes, G., Gottlöber, S., & Springel, V. 2006, MNRAS, 371, 401
Hoffman, Y., Metuki, O., Yepes, G., et al. 2012, MNRAS, 425, 2049
Iliev, I. T., Ciardi, B., Alvarez, M. A., et al. 2006, MNRAS, 371, 1057
Iliev, I. T., Mellema, G., Shapiro, P. R., & Pen, U.-L. 2007, MNRAS, 376, 534
Iliev, I. T., Moore, B., Gottlöber, S., et al. 2011, MNRAS, 413, 2093
Iliev, I. T., Shapiro, P. R., Ferrara, A., & Martel, H. 2002, ApJL, 572, L123
Iliev, I. T., Shapiro, P. R., & Raga, A. C. 2005, MNRAS, 361, 405
Iliev, I. T., Whalen, D., Mellema, G., et al. 2009, MNRAS, 400, 1283
Irwin, M. J., Belokurov, V., Evans, N. W., et al. 2007, ApJL, 656, L13
Kim, H.-S., Wyithe, J. S. B., Raskutti, S., Lacey, C. G., & Helly, J. C. 2013, MNRAS, 428, 2467
Klypin, A., Kravtsov, A. V., Valenzuela, O., & Prada, F. 1999, ApJ, 522, 82
Knebe, A., Libeskind, N. I., Doumler, T., et al. 2011a, MNRAS, 417, L56
Knebe, A., Libeskind, N. I., Knollmann, S. R., et al. 2011b, MNRAS, 412, 529
Knollmann, S. R., & Knebe, A. 2009, ApJS, 182, 608
Kogut, A., Spergel, D. N., Barnes, C., et al. 2003, ApJS, 148, 161
Koposov, S. E., Yoo, J., Rix, H., et al. 2009, ApJ, 696, 2179
Li, T. Y., Alvarez, M. A., Wechsler, R. H., & Abel, T. 2013, arXiv:1306.2971
Li, Y., De Lucia, G., & Helmi, A. 2010, MNRAS, 401, 2036
Libeskind, N. I., Hoffman, Y., Knebe, A., et al. 2012, MNRAS, 421, L137
Libeskind, N. I., Knebe, A., Hoffman, Y., Gottlöber, S., & Yepes, G. 2011a, MNRAS, 418, 336
Libeskind, N. I., Knebe, A., Hoffman, Y., et al. 2011b, MNRAS, 411, 1525

Libeskind, N. I., Yepes, G., Knebe, A., et al. 2010, MNRAS, 401, 1889
Macciò, A. V., Kang, X., Fontanot, F., et al. 2010, MNRAS, 402, 1995
Martin, N. F., Ibata, R. A., Bellazzini, M., et al. 2004, MNRAS, 348, 12
Moore, B., Ghigna, S., Governato, F., et al. 1999, ApJL, 524, L19
Muñoz, J. A., Madau, P., Loeb, A., & Diemand, J. 2009, MNRAS, 400, 1593
Ocvirk, P., & Aubert, D. 2011, MNRAS, 417, L93
Ocvirk, P., & Aubert, D. 2012, in EPJ Web of Conferences, Vol. 19, Assembling the Puzzle of the Milky Way, ed. C. Reylé, A. Robin, & M. Schultheis (Les Ulis Cedex: EDP Sciences), 3005
Ocvirk, P., Pichon, C., & Teyssier, R. 2008, MNRAS, 390, 1326
Pawlik, A. H., & Schaye, J. 2011, MNRAS, 412, 1943
Petkova, M., & Springel, V. 2011, MNRAS, 412, 935
Rasera, Y., & Teyssier, R. 2006, A&A, 445, 1
Razoumov, A. O., & Sommer-Larsen, J. 2010, ApJ, 710, 1239
Rosdahl, J., & Blaizot, J. 2012, MNRAS, 423, 344
Shapiro, P. R., Iliev, I. T., & Raga, A. C. 2004, MNRAS, 348, 753
Spergel, D. N., Bean, R., Doré, O., et al. 2007, ApJS, 170, 377
Springel, V. 2005, MNRAS, 364, 1105
Springel, V., & Hernquist, L. 2003, MNRAS, 339, 289
Walsh, S. M., Jerjen, H., & Willman, B. 2007, ApJL, 662, L83
Weinmann, S. M., Macciò, A. V., Iliev, I. T., Mellema, G., & Moore, B. 2007, MNRAS, 381, 367
Willman, B., Dalcanton, J. J., Martinez-Delgado, D., et al. 2005, ApJL, 626, L85
Wise, J. H., & Abel, T. 2011, MNRAS, 414, 3458
Wise, J. H., & Cen, R. 2009, ApJ, 693, 984
Yajima, H., Choi, J.-H., & Nagamine, K. 2011, MNRAS, 412, 411
Zahn, O., Lidz, A., McQuinn, M., et al. 2007, ApJ, 654, 12
Zucker, D. B., Belokurov, V., Evans, N. W., et al. 2006, ApJL, 643, L103